BAO angular scale at z_{eff} = 0.11 with the SDSS blue galaxies

E. de Carvalho[1,2]⋆, A. Bernui[2], F. Avila[2], C. P. Novaes[3], and J. P. Nogueira-Cavalcante[2]

[1] Centro de Estudos Superiores de Tabatinga, Universidade do Estado do Amazonas, 69640-000, Tabatinga, AM, Brazil

[2] Observatório Nacional, Rua General José Cristino 77, São Cristóvão, 20921-400 Rio de Janeiro, RJ, Brazil

[3] Instituto Nacional de Pesquisas Espaciais, Av. dos Astronautas 1758, Jardim da Granja, São José dos Campos, SP, Brazil

May 6, 2021

ABSTRACT

Aims. We measure the transverse baryon acoustic oscillations (BAO) signal in the local Universe using a sample of blue galaxies from the Sloan Digital Sky Survey (SDSS) survey as a cosmological tracer.
Methods. The method is weakly dependent on a cosmological model and is suitable for 2D analyses in thin redshift bins to investigate the SDSS data in the interval $z \in [0.105, 0.115]$.
Results. We detect the transverse BAO signal $\theta_{\text{BAO}} = 19.8° \pm 1.05°$ at $z_{\text{eff}} = 0.11$, with a statistical significance of $2.2\,\sigma$. Additionally, we perform tests that confirm the robustness of this angular BAO signature. Supported by a large set of log-normal simulations, our error analyses include statistical and systematic contributions. In addition, considering the sound horizon scale calculated by the Planck Collaboration, r_s^{Planck}, and the θ_{BAO} value obtained here, we obtain a measurement of the angular diameter distance $D_A(0.11) = 258.31 \pm 13.71\,h^{-1}$Mpc. Moreover, combining this θ_{BAO} measurement at low redshift with other BAO angular scale data reported in the literature, we perform statistical analyses for the cosmological parameters of some Lambda cold dark matter (ΛCDM) type models.

Key words. Cosmological parameters – Large-scale structure of Universe – Observations

1. Introduction

Embedded in the 3D distribution of cosmic luminous matter are geometrical signatures from the primordial baryon acoustic oscillations (BAO; Peebles & Yu 1970; Sunyaev & Zeldovich 1970; Bond & Efstathiou 1987; Eisenstein et al. 2005; Cole et al. 2005). They can be statistically revealed in large-scale and numerically dense astronomical surveys and are used as a standard ruler to measure our distance to the data region. These analyses are performed by studying different cosmological tracers from a variety of astronomical surveys, such as the Sloan Digital Sky Survey (SDSS), the 6dF Galaxy Survey, and the WiggleZ Dark Energy Survey (Alam et al. 2017, 2020; Beutler et al. 2011; Blake et al. 2011). A set of precise distance measurements for several redshift values will unambiguously describe the dynamics of the universe (Eisenstein & Hu 1998; Bassett & Hlozek 2010; Eisenstein et al. 2007).

The BAO distance measurements are obtained using two-point statistics in at least two ways. The first approach, based on the 3D information, assumes a fiducial cosmology to transform the redshift of each cosmic object into its radial distance, and with the two angular coordinates measured in the survey, the comoving distance between all possible pairs is calculated to construct the two-point correlation function (2PCF). The BAO signal obtained with this approach determines the sound horizon scale at the end of the baryon drag epoch, r_s, and the spherically averaged distance D_V (Beutler et al. 2011; Blake et al. 2011; Alam et al. 2017; Abbott et al. 2019). The second approach uses 2-dimensional (2D) information: the data in a redshift shell are projected on the celestial sphere. With the two angular coordi-

nates of each cosmic object, the angular separation between pairs is then calculated and the two-point angular correlation function (2PACF) is calculated, where the BAO angular scale provides a measure of the angular diameter distance D_A if r_s is known. To minimize projection effects that would affect this measurement, the data should be in a thin redshift shell (Sánchez et al. 2011; Carnero et al. 2012; Carvalho et al. 2016).

In addition to the advantages and disadvantages of each approach, the 2D method is a quasi model-independent procedure, with a weak dependence on the fiducial cosmology that we explained below. We adopt it here to measure the BAO angular scale θ_{BAO}. The 2D approach was not widely applied to early data releases because the number density of cosmic objects was not high enough to provide a good BAO signal-to-noise ratio (S/N) in thin redshift shells. However, the current data releases have suitably increased this quantity. Several studies reported 2D BAO measurements using luminous red galaxies (LRG) and quasar samples at several redshifts (Sánchez et al. 2011; Carnero et al. 2012; Salazar et al. 2017; Carvalho et al. 2016; Abbott et al. 2019; de Carvalho et al. 2018). The present work extends these analyses with a 2D BAO measurement at low redshift, $z_{\text{eff}} = 0.11$ from an unusual cosmological tracer, the SDSS sample of blue galaxies (York et al. 2000; Avila et al. 2019).

This work is organized as follows. Section 2 provides the details of the blue galaxy sample selection from the SDSS data set, the generation of the random catalog, and the simulations we used. Section 3 describes the statistical tools employed in the 2D clustering analyses. In Sect. 4 we describe our main results, giving details on the 2D analyses and our estimate of the BAO angular scale, while in Sect. 5 we present the discussion of our results and final conclusions.

⋆ edfilho@uea.edu.br

2. Data description

2.1. Blue galaxy sample and random catalogs

We used the sample of blue star-forming galaxies analyzed in Avila et al. (2019). The selected data are part of the twelfth public data release, DR12, of the SDSS collaboration (Alam et al. 2015). We considered the low-redshift SDSS blue galaxies displayed in the north galactic cap with the footprint observed in Fig. 1, covering an area of $\sim 7,000$ deg^2.

To optimize between sample variance and shot noise, the galaxy field has to be weighted. To do this, we assigned weights to each galaxy based on the average local density in the analyzed region by using the Feldman-Kaiser-Peacock (FKP) weights (Feldman et al. 1994). This is a scale-independent weighting that depends on redshift, $w_{FKP}(z) = 1/(1 + n(z)P_0)$, where P_0 is the amplitude of the power spectrum and $n(z)$ is the number density of galaxies. We used $P_0 \simeq 10,000\,h^{-3}\mathrm{Mpc}^3$, the power amplitude relevant to the BAO signal $k \approx 0.15h\mathrm{Mpc}^{-1}$ (Eisenstein et al. 2005; Beutler et al. 2011; Carter et al. 2018). Therefore the effective redshift of our sample, z_{eff}, calculated with the FKP galaxy weights, $w_i \equiv w(z_i) = w_{FKP}(z_i)$, is obtained through (see, e.g., Carter et al. 2018)

$$z_{eff} = \frac{\sum_{i=1}^{N_g} w_i\, z_i}{\sum_{i=1}^{N_g} w_i}\,, \tag{1}$$

where N_g is the total number of galaxies in the sample.

We searched for a statistically significant angular BAO detection at the lowest redshift. After analyzing bins with a large number of galaxies (to minimize the statistical noise) that are located in a thin redshift bin (to minimize the nonlinear contributions due to the projection effect, see, e.g., Sánchez et al. (2011)), we selected the data sample contained in the thin redshift bin $0.105 \leq z \leq 0.115$, with $\delta z = 0.01$ and $z_{eff} = 0.11$. This bin contains $N_g = 15,942$ blue galaxies.

We would like to point out that the comoving volume survey containing these $N_g = 15,942$ blue galaxies is $V \simeq 0.0063\,(\mathrm{Gpc}/h)^3$. This seems to be a small volume in which to look for a transverse BAO signal, but the important parameter for these analyses is the number density n. For this sample of blue galaxies, the number density is $n = N_g/V \simeq 2.5 \times 10^6 (h/\mathrm{Gpc})^3$. For comparison, $n_{LRG} = 10^4 - 10^5\,(h/\mathrm{Gpc})^3$ for the SDSS LRG sample analyzed in the 3D BAO detection (Eisenstein et al. 2005), or $n_{quasars} \simeq 7.3 \times 10^3\,(h/\mathrm{Gpc})^3$ for the 2D BAO detection using a sample of SDSS quasars (de Carvalho et al. 2018).

The random catalogs are an important ingredient in our analyses. They are necessary to extract the BAO features from the data. For this, they must have properties in common to those observed in the SDSS blue galaxy catalog. We produced 50 random catalogs for the 2D analyses (with $N_{sim} \simeq 16,000$ in each catalog) with Poisson-distributed objects (Peebles & Hauser 1974) sharing the observational features of the data set in analyses (i.e., the same number density and footprint sky area as the SDSS data). Our set of random catalogs was produced following the method described in the Appendix B of de Carvalho et al. (2018), where they were satisfactorily tested through a null test analysis (see, e.g., Sect. 5 of Landy & Szalay 1993) to confirm that they do not introduce spurious signals.

2.2. Log-normal simulations

To estimate the error bars of the 2PACF and the statistical significance of our results, we used the covariance matrix built
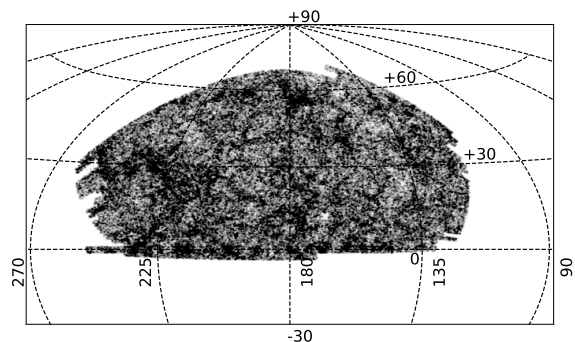
Fig. 1. Sample of SDSS blue galaxies in equatorial coordinates J2000 (in degrees).

from full-sky log-normal simulations that we produced with the `FLASK` code[1] (Xavier et al. 2016; de Carvalho et al. 2020). We generated a set of 1,000 simulations for which we assume the Lambda cold dark matter (ΛCDM) cosmological parameters measured by the Planck Collaboration (2020), including all effects available such as lensing, redshift space distortions (RSD), and nonlinear clustering to compute with the code `CAMBsources`[2] (Challinor & Lewis 2011) the fiducial angular power spectrum C_ℓ that was used as input.

This set of simulations was designed to be used in the angular analyses where we assumed a top-hat redshift bin ($0.105 \leq z \leq 0.115$) with a surface number density of 2.3 galaxies *per* deg^2 (the same as in SDSS data). These simulated data share the observational features of the data set in the analyses, that is, the same number density and footprint sky area, and they were also weighted by the FKP scheme. The number of simulated cosmic objects in each catalog is $N_{sim} \simeq 16,000$. For this set of simulated maps, we adopted an angular resolution of 0.11 deg^2, given by the `HEALPix`[3] (Górski et al. 2005) parameter $N_{side} = 512$.

3. Two-point correlation estimator

We performed a 2D BAO measurement at low redshift with the SDSS blue galaxy sample. This measurement complements similar 2D analyses performed following the same method applied to other cosmological tracers, such as LRG and quasars, at several redshifts (Carvalho et al. 2016; Alcaniz et al. 2017; de Carvalho et al. 2018; Carvalho et al. 2020). The 2D BAO studies were performed by applying the 2PACF to the thin redshift bin $0.105 \leq z \leq 0.115$. Additionally, supported by a large set of lognormal simulations, we describe how the covariance matrix was used in the error analyses, including statistical and systematic contributions.

3.1. Two-point angular correlation function

In the 2D analysis, the 2PACF (Peebles & Yu 1970; Landy & Szalay 1993) estimates the angular correlation for data pairs projected on the celestial sphere (for alternative clustering analyses, see, e.g., Avila et al. 2018, 2019; Bengaly et al. 2017; Feldbrugge et al. 2019; Novaes et al. 2016, 2018; Marques & Bernui 2020a; Marques et al. 2020b; Pandey & Sarkar 2020; Sosa & Niz 2020).

---

[1] `http://www.astro.iag.usp.br/~flask`
[2] `https://camb.info/sources/`
[3] `https://healpix.sourceforge.io/`

Considering blue galaxies in a redshift shell, the 2PACF measures the angular diameter distance D_A due to the transverse BAO signal of the sound horizon scale there, where this signature appears as a bump at certain angular scale. The expression for the 2PACF estimator, $\omega(\theta)$, is given by

$$\omega(\theta) \equiv \frac{DD(\theta) - 2DR(\theta) + RR(\theta)}{RR(\theta)}, \qquad (2)$$

with θ the angular separation between any pair of blue galaxies A, B, given by

$$\theta = \arccos[\sin \delta_A \sin \delta_B + \cos \delta_A \cos \delta_B \cos(\alpha_A - \alpha_B)],$$

where α_A, α_B and δ_A, δ_B are the right ascension and declination coordinates of the blue galaxies A and B, respectively (Landy & Szalay 1993; Sánchez et al. 2011).

To find the angular scale θ_{FIT} of the BAO bump in the 2PACF, $\omega(\theta)$, we used the method proposed by Sánchez et al. (2011), which is based on the empirical parameterization of $\omega = \omega(\theta)$,

$$\omega(\theta) = A + B \theta^\gamma + C \exp^{-(\theta-\theta_{\text{FIT}})^2/2\sigma_{\text{FIT}}^2}, \qquad (3)$$

where A, B, γ, C, θ_{FIT}, and σ_{FIT} are free parameters. Therefore this equation provides the BAO bump best-fit, θ_{FIT}, and the width of the bump is σ_{FIT}.

The final measurement of the acoustic peak was obtained after accounting for the shift due to the projection effect (Sánchez et al. 2011; Carnero et al. 2012; Carvalho et al. 2016). In the 2D analyses, all galaxies in the redshift bin in the study with thickness δz are assumed to be projected onto the celestial sphere. Thus, the finite thickness of the shell, $\delta z \neq 0$, produces a shift of the BAO peak. This shift is estimated through numerical analysis by assuming a fiducial cosmology (as we show in Sect. 4.2), but the results show that for thin shells, the shift is small and weakly dependent on the cosmological parameters (for details, see, e.g., Sánchez et al. 2011; Carvalho et al. 2016). The redshift shell should be as thin as possible to minimize the projection effect that affects the measurement by erasing the acoustic signature, but at the same time, it should be a numerically dense data set, enough to obtain a good BAO S/N. We calculate the shift to be applied to θ_{FIT} due the projection effect in Sect. 4.2.

### 3.2. Covariance matrix estimation

To estimate the covariance matrix and the significance of our results, we used the galaxy mocks described above (see Sect. 2.2). For each mock, we extracted the 2PACF information from a set of N_b bins in which the interval of θ values was divided. The covariance matrix for $\omega(\theta)$ was estimated using the expression

$$\text{Cov}_{ij} = \frac{1}{N} \sum_{k=1}^{N} \left[w_k(\theta_i) - \overline{w}(\theta_i) \right] \left[w_k(\theta_j) - \overline{w}(\theta_j) \right], \qquad (4)$$

where the i and j indices represent each θ bin, $i, j = 1, \ldots, N_b$, and w_k is the 2PACF for the k-th mock catalog, with $k = 1, \ldots, N$; $\overline{w}(\theta_i)$ is the mean value for this statistics over the $N = 1,000$ mocks in that bin. Finally, the error of $w(\theta_i)$ is the square root of the main diagonal, $\Delta w(\theta_i) = \sqrt{\text{Cov}_{ii}}$.

4. Clustering analyses in 2D

We studied the clustering of the SDSS blue galaxy sample performing 2D analysis. Using the estimator given by Eq. (2),
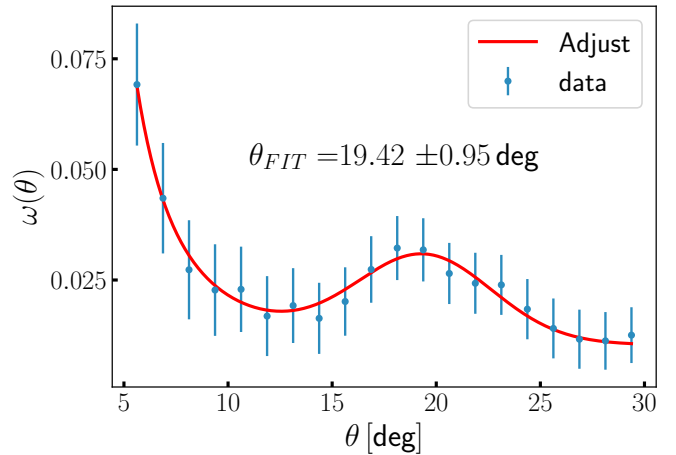
Fig. 2. BAO signature obtained in the 2PACF by analyzing the sample in the redshift interval $z \in [0.105, 0.115]$, with $\delta z = 0.01$. The bin size in this 2PACF is $1.25°$, and we use 50 random catalogs with the same observational features as the galaxy catalog.

Parameters	Equation (3)
A	$9.92 \pm 6.41 \; (\times 10^{-3})$
B	$0.77 \pm 2.05 \; (\times 10^{-4})$
γ	2.86 ± 1.06
C	$19.29 \pm 7.43 \; (\times 10^{-3})$
σ_{FIT}	$3.26° \pm 0.96°$
θ_{FIT}	$19.42° \pm 0.95°$ (stat)

Table 1. Best-fit parameters of Eq. (3), obtained through the χ^2 statistics, Eq. (5), using the covariance matrix shown in Fig. 3.

$\omega(\theta)$, we calculated the 2PACF for our sample of $N_g = 15,942$ galaxies in the redshift interval $z \in [0.105, 0.115]$, with effective redshift $z_{\text{eff}} = 0.11$. The 2PACF was calculated using TREECORR (Jarvis et al. 2004) for equally spaced values of θ in the interval $5° \leq \theta \leq 30°$, in a total of $N_b = 20$ bins, which means that the bin size was $1.25°$. To extract the BAO bump position, we used Eq. (3) to fit the 2PACF data through a least-squares method; the errors in the parameters correspond to the statistical uncertainties provided by the fitting procedure (the estimated covariance matrix of the parameters). The result is shown in Fig. 2, where $\theta_{\text{FIT}} = 19.42°$. Our result for this procedure is summarized in Table 1, where we display the best-fit parameters obtained in this fitting approach using Eq. (3).

4.1. Statistical significance

The statistical significance of the BAO angular measurement was obtained through the χ^2 method,

$$\chi^2(\alpha) = \left[w - w^{\text{FIT}}(\alpha) \right]^T \text{Cov}^{-1} \left[w - w^{\text{FIT}}(\alpha) \right], \qquad (5)$$

where we used the inverse of the covariance matrix, Cov, estimated as described in Sect. 3.2 and shown in Fig. 3. The symbols [ ] and [ ]^T represent column vectors and row vectors, respectively.

Following de Carvalho et al. (2018), we adjusted the parameters of Eq. (3) based on the minimum χ^2 method for $\alpha \in$
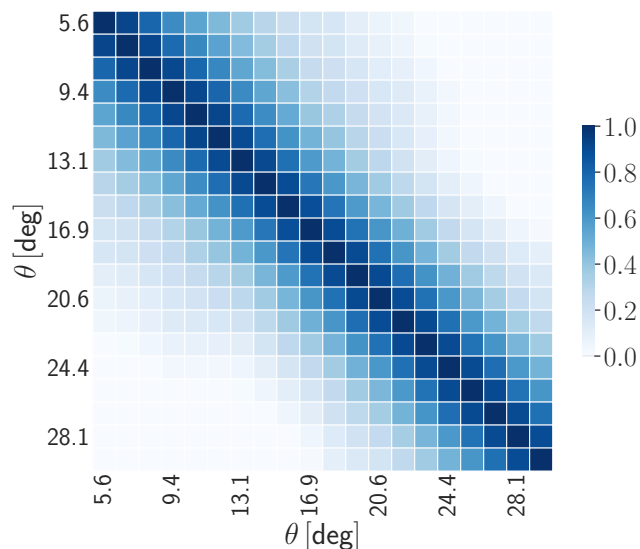
Fig. 3. Covariance matrix for the 2PACF obtained from Eq. (4) using the set of log-normal simulated maps (see Sect. 2.2).

[0.85, 1.25], which is called the scale dilation parameter, for two cases: considering C as free parameter, $C \neq 0$ ($\chi^2_{min} = 13.13$), and imposing $C = 0$ ($\chi^2_{min} = 22.06$), where χ^2_{min} corresponds to $\alpha_{min} = 0.996$, the latter case representing the non-BAO case. Table 1 shows the best-fit parameters obtained considering $\alpha = 1$.

As a result, the best-fit[4] of the non-BAO case (16 degrees of freedom, dof), compared to the BAO case (13 dof), is disfavored by $\Delta\chi^2 = 8.93$. Therefore our BAO angular detection has a statistical significance of $2.2\,\sigma$, which is compatible with the distance of the C parameter from zero.

4.2. Projection effect in the 2PACF

To know the angular scale θ_{BAO}, we need to correct the θ_{FIT} due to the projection effect, which produces a shift in the BAO bump position (Sánchez et al. 2011). To quantify this shift, we first computed the expected angular BAO scale, θ^0_E, corresponding to the bump position for the case $\delta z = 0$ calculated from the expected 2PACF,

$$w_E(\theta, z) = \int_0^\infty dz_1\, \phi(z_1) \int_0^\infty dz_2\, \phi(z_2)\, \xi_E(s, z), \qquad (6)$$

where $z = z_{eff} = (z_1 + z_2)/2$, with $z_2 = z_1 + \delta z$, and $\phi(z_i)$ is the normalized galaxy selection function at redshift z_i. The function ξ_E is the 2PCF expected in the fiducial cosmology, given by (see, e.g., Sánchez et al. 2011)

$$\xi_E(s, z) = \int_0^\infty \frac{dk}{2\pi^2}\, k^2\, j_0(ks)\, b^2\, P_m(k, z), \qquad (7)$$

where j_0 is the zeroth-order Bessel function, $P_m(k, z)$ is the matter power spectrum, and b is the bias factor.

It is suitable to examine the RSD effect on the measurement of the angular BAO signature. For this we performed analyses that included the linear RSD by changing $P_m(k, z)$ by

---

[4] Here α is also accounted for as a free parameter, that is, we have a total of four and seven free parameters in the non-BAO and BAO cases, respectively.

$(1 + \beta\mu^2)^2 P_m(k, z)$ in the Eq. (7), where we considered two cases: the linear, $P^L_m(k, z)$, and the nonlinear, $P^{NL}_m(k, z)$, matter power spectra produced using the numerical code CAMB (Challinor & Lewis 2011), at $z = 0.11$. We assumed the ΛCDM model with the cosmological parameters measured by the Planck Collaboration (2020). The term $(1 + \beta\mu^2)^2$ corresponds to the Kaiser model for large-scale RSD (Kaiser 1987), where β, the velocity scale parameter is $\beta = f/b$, b is the linear bias, and f is the growth rate of cosmic structures, with $f \simeq \Omega_m(z)^{0.55}$, where μ is the cosine of the angle between the wave vector **k** and the line of sight.

Our results show that the relative difference in the bump position between the linear matter power spectra with and without the linear RSD is 0.84 %. For the nonlinear matter power spectra with and without the linear RSD, the relative difference in the bump position is equal to 0.70 %. On the other hand, comparing the linear and the nonlinear matter power spectra cases, the differences in the bump position are 0.14 % and 0.00 % for the cases with and without the linear RSD effect, respectively. In all cases the relative differences are smaller than 1 %, therefore we conclude that these effects on our angular BAO measurement are small and are included in the final error.

Next, we applied this procedure to our data, where $\delta z = 0.01$ is the thickness of the redshift bin used here, to find $\theta^{\delta z}_E$. Then, the BAO angular scale, θ_{BAO}, is

$$\theta_{BAO}(z) = \theta_{FIT}(z) + \Delta\theta(z, \delta z)\, \theta_{FIT}(z), \qquad (8)$$

where $\Delta\theta(z, \delta z) \equiv (\theta^0_E - \theta^{\delta z}_E)/\theta^0_E$ shifts the fitted value $\theta_{FIT}(z)$ to the correct acoustic scale $\theta_{BAO}(z)$, at $z = z_{eff} = 0.11$.

Assuming the ΛCDM model with the cosmological parameters measured by Planck Collaboration (2020), we estimate $\theta^0_E = 17.93°$ and $\theta^{0.01}_E = 17.58°$, which corresponds to $\Delta\theta = 1.96\%$. Consequently, $\theta_{BAO}(z_{eff} = 0.11) = 19.8°$. As shown by Sánchez et al. (2011), the choice of the fiducial cosmological model introduces a systematic error of 1% in the final θ_{BAO} error.

4.3. Robustness of the BAO signal

We performed a robustness test in the two-point angular correlation statistics to confirm the BAO signature in the 2PACF. To verify that the BAO signature corresponds to a robust detection, we performed the small-shifts criterion test (Carvalho et al. 2016; de Carvalho et al. 2018). The main idea here is to distinguish between the true BAO bump, which is expected to be smoothed, but survives, under weak perturbations in the galaxy positions, while other local maxima that originate in systematic effects or statistical noise tend to disappear in a reanalysis after the perturbations. For this, we first generated 100 modified galaxy catalogs by drawing the modified position of each galaxy resulting from a random Gaussian distribution with the mean equal to the original position and standard deviation σ_s, and for each modified catalog we calculated the 2PACF curve. The final 2PACF was estimated as the average over the 100 curves resulting from each of the modified galaxy catalogs, perturbed considering the standard deviation σ_s. We performed this process for the cases with $\sigma_s = 1.0°, 2.0°$, and $3.0°$. In the calculation of each 2PACF we used the same set of 50 random catalogs as in the main analysis, always applying Eq. (2).

Our results are shown in Fig. 4, where we present the original data as black dots together with the three cases for σ_s that are printed as solid colored curves. As observed, the larger the random displacements in the blue galaxy angular po-
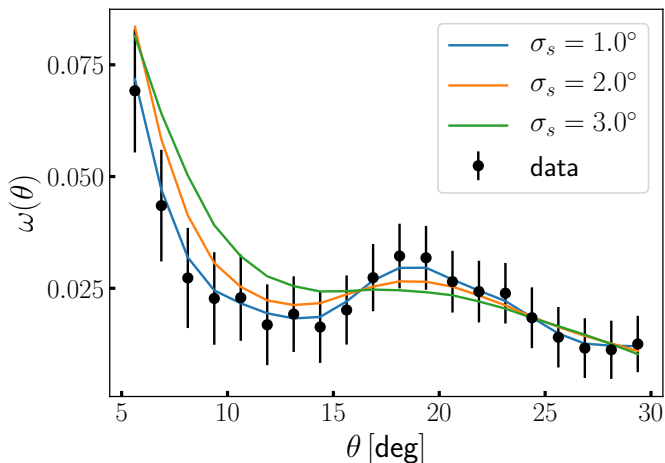
Fig. 4. Robustness test analyses. We performed small random shifts in the galaxies angular coordinates and repeated the 2PACF calculation. The black dots represent the original data analysis, and the curves correspond to the cases we studied (as indicated in the legend).

sitions, the smoother the 2PACF curves. This also smoothes the BAO bump signature. Simultaneously, these displacements also smooth other maxima and minima that may originate from systematic effects or statistical noise and appear in the original 2PACF.

4.4. Spectroscopic-z error

As shown by Sánchez et al. (2011), the main source of error in the BAO signal for photometric surveys is the uncertainty in the measurement of the redshift, z. Although we study spectroscopic data, for which this uncertainty is smaller, it is important to quantify this source of error in the final BAO measurement. To do this, we constructed 300 spec-z simulations for which we considered the measured z of each blue galaxy as the true one plus a random error obtained from a Gaussian distribution of zero mean and standard deviation given by its measured uncertainty that is available in the data catalog (see de Carvalho et al. 2020).

The results of this analysis are displayed in Fig. 5. There we show the histogram of the relative difference between the $\theta_{\rm FIT}$ measured for each spec-z simulation and the $\theta_{\rm FIT}$ from the blue galaxy data. As expected, in the case of spectroscopic data as for the blue galaxy data analyzed here, the error coming from the z-uncertainty introduces a small error in the final angular BAO measurement of 0.11%.

The 2D BAO measurement performed here complements a set of other measurements obtained with the same method (Carvalho et al. 2016; Alcaniz et al. 2017; de Carvalho et al. 2018; Carvalho et al. 2020). Thus, our angular BAO measurement at $z_{\rm eff} = 0.11$ is $\theta_{\rm BAO} = 19.8° \pm 1.05°$. This error in the $\theta_{\rm BAO}$ measurement includes the statistical and systematic errors due to the spectroscopic-z error, parameterization, RSD, projection effect, and nonlinearities (see Sánchez et al. 2011, for a broader discussion of the error estimation).
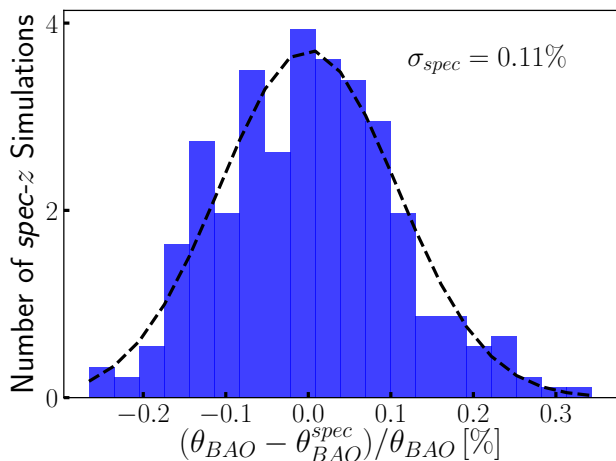
Fig. 5. Histogram of the relative difference, in percentage (%), between the BAO scale obtained from the blue galaxy data, $\theta_{\rm BAO}$, and those obtained from each simulated spec-z catalog, $\theta_{\rm BAO}^{spec}$. As expected, for the spectroscopic data the z errors affect the measurements of the BAO signature little. They contribute to the final error with only 0.11%.

4.5. Cosmological constraints from $\theta_{\rm BAO}$ data

Here we combined our 2D measurement of the BAO scale at low redshift, $z_{\rm eff} = 0.11$, with the results obtained by Carvalho et al. (2016), Alcaniz et al. (2017), de Carvalho et al. (2018) and Carvalho et al. (2020) (see Fig. 6), to constrain the parameters of the ΛCDM, wCDM, and $w(t)$CDM models. For the $w(t)$CDM model we chose the Barboza-Alcaniz parameterization (Barboza & Alcaniz 2008). To be consistent with the error determination from the analyses mentioned above and to allow a proper combination of the results, in this section we adopt $\sigma_{\rm BAO} = \sigma_{\rm FIT} = 3.26°$ as the error in the measurement of $\theta_{\rm BAO}$, that is, $\theta_{\rm BAO}(0.11) = 19.8° \pm 3.26°$.
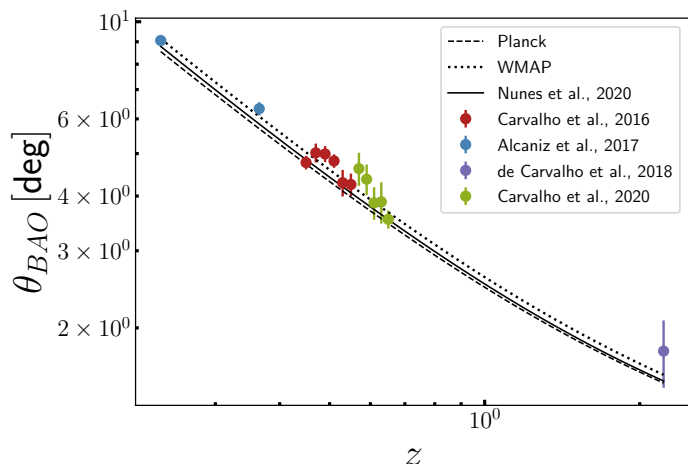
To restrict the cosmological parameters of the models ΛCDM, wCDM, and $w(t)$CDM, we performed Markov chain Monte Carlo (MCMC) analyses to explore the parameter space. In all cases we assumed $\Omega_k = 0$. The analyses were performed using the code PyMC[5], assuming uniform priors for all the parameters in study except for r_s, for which we assumed a Gaussian prior with a standard deviation equal to the measurement error. We investigated three different values of r_s: $r_s = 99.08 \pm 0.18\,h^{-1}$Mpc obtained by the Planck Collaboration (2020), $r_s = 106.61 \pm 3.47\,h^{-1}$Mpc calculated by Hinshaw et al. (2013) (WMAP team), and $r_s = 102.2 \pm 0.2\,h^{-1}$Mpc calculated by Nunes et al. (2020a). The results of these analyses are displayed in Table 2, where the uncertainties correspond to $1\,\sigma$ errors. Figure 7 shows the constraints for ΛCDM model case as an example. The inner and the outer curves represent the $1\,\sigma$ and $2\,\sigma$ contour levels, respectively [6]. In the histogram plots, the $\pm 1\,\sigma$ values are shown as dashed vertical lines. In all cases, the data prefer a high fraction of matter, with $\Omega_m > 0.4$. Moreover, the results from the wCDM and $w(t)$CDM models are consistent with the ΛCDM model, although the analyses reveal a poorer constraint of the parameters.

In general, we observe that the results are consistent with each other, but when the value from the Planck Collaboration, $r_s = 99.08 \pm 0.18\,h^{-1}$Mpc, is used as a prior for r_s, the constraints

---

[5] https://pymc-devs.github.io/pymc
[6] This figure was made using the Corner Plot software developed by Foreman-Mackey (2016).

Fig. 6. θ_{BAO} measurements as a function of redshift. When the ΛCDM model is assumed, the dashed, dotted, and continuous lines represent the results obtained using the cosmological parameters from Planck Collaboration (2020), Hinshaw et al. (2013) (WMAP team), and Nunes et al. (2020a), respectively.

show the largest error bars (see Table 2). According to our tests, they are probably due to the small error of this parameter.

Finally, we calculated the angular diameter distance at $z_{\text{eff}} = 0.11$. The angular scale of the BAO bump, $\theta_{\text{BAO}}(z)$, is related to the angular diameter distance $D_A(z)$ and the sound horizon r_s by

$$D_A(z) = \frac{r_s}{(1 + z)\,\theta_{\text{BAO}}(z)} \; . \tag{9}$$

When we use our angular BAO measurement, $\theta_{\text{BAO}}(0.11) = 19.8° \pm 1.05°$, and the sound horizon scale calculated by the Planck Collaboration (2020), $r_s = 99.08 \pm 0.18\,h^{-1}\text{Mpc}$, we use Eq. (9) to determine the angular diameter distance at $z_{\text{eff}} = 0.11$: $D_A(0.11) = 258.31 \pm 13.71\,h^{-1}\text{Mpc}$.

5. Conclusions

The availability of a rich set of astronomical data, mapping diverse cosmological tracers in various redshift intervals observed in large sky regions during long-time surveys makes these times exciting. This motivated us to study the BAO phenomenon in the local Universe, performing 2D statistical analyses of the low-redshift blue galaxy sample from the SDSS-DR12.

In the 2D clustering analyses performed here, we used a sample containing $N_g = 15,942$ blue galaxies in the thin redshift bin $z \in [0.105, 0.115]$ with $z_{\text{eff}} = 0.11$. Applying the 2PACF estimator on these data, we measured the transverse BAO signature at $\theta_{\text{BAO}}(0.11) = 19.8° \pm 1.05°$ with a statistical significance of $2.2\,\sigma$. Our error analyses included statistical and systematic contributions. We also performed analyses that confirm the robustness of this transverse BAO measurement (see Sect. 4.3 for details).

Additionally, we used the sound horizon scale calculated by the Planck Collaboration (2020), $r_s = 99.08 \pm 0.18\,h^{-1}\text{Mpc}$, to obtain a measurement of the angular diameter distance. Using this value of r_s and our result for the BAO angular scale $\theta_{\text{BAO}}(0.11)$ in Eq. (9), we obtained a measurement of the angular diameter distance at $z_{\text{eff}} = 0.11$: $D_A(0.11) = 258.31 \pm 13.71\,h^{-1}\text{Mpc}$. For the error analyses, which requires the computation of the covariance matrices, we used a set of log-normal
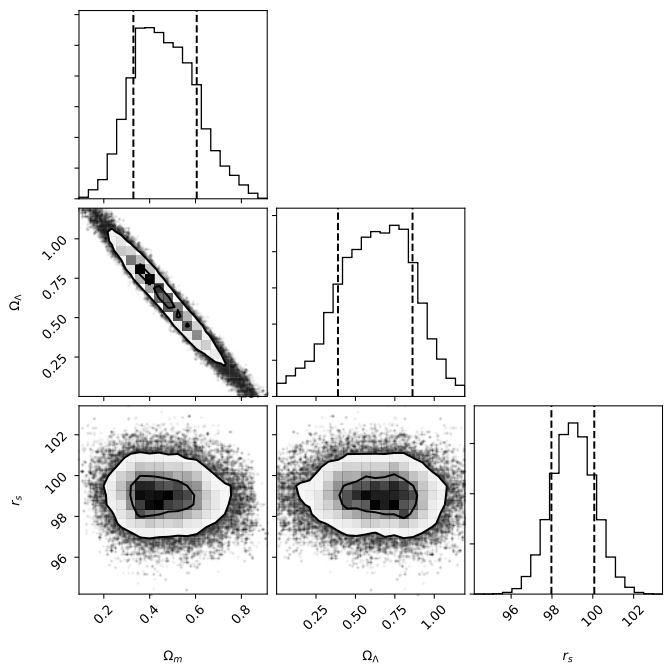
Fig. 7. Contour levels at $1\,\sigma$ (inner) and $2\,\sigma$ (outer) for the Ω_m, Ω_Λ and r_s parameters extracted from the BAO angular scale data and the r_s prior defined from the Planck value of Planck Collaboration (2020), namely $r_s = 99.08 \pm 0.18\,h^{-1}\text{Mpc}$. In the histogram plots, the dashed vertical lines represent the $\pm 1\,\sigma$ values.

simulations with similar observational features as the SDSS data we analyzed, including effects such as lensing, RSD, and non-linear clustering (see Sect. 2.2 for details).

Our measurement of $D_A(0.11)$ was obtained by applying a method that is weakly dependent on a cosmological model, exactly as other measurements of $D_A(z)$ were obtained (Carvalho et al. 2016; Alcaniz et al. 2017; de Carvalho et al. 2018; Carvalho et al. 2020). Here we used these measurements to perform MCMC analyses that constrain cosmological parameters of some ΛCDM-type models, namely ΛCDM itself, wCDM, and $w(t)$CDM. The results we obtained are shown in Table 2 and Fig. 7. They agree with the reported values for these models (for analyses of cosmological parameters, see, e.g., Hinshaw et al. 2013; Planck Collaboration 2020; Marques et al. 2019; Nunes et al. 2020a,b).

References

Abbott, T., Abdalla, F., Alarcon, A., et al. 2019, MNRAS, 483, 4866

Alam, S., Albareti F. D., Prieto C. A., et al. 2015, ApJS, 219, 12

Alam, S., Ata, M., Bailey, S., et al. 2017, MNRAS, 470, 2617

Alam, S. et al., 2020, arXiv:2007.08991

Alcaniz, J. S., et al. 2017, Gravity and the Quantum, Fundamental Theories of Physics, 187, 11

Avila, F., Novaes, C. P., Bernui, A., & de Carvalho, E. 2018, J. Cosmology Astropart. Phys., 12, 041

Avila, F., Novaes, C. P., Bernui, A., de Carvalho, E., & Nogueira-Cavalcante, J. P. 2019, MNRAS, 488, 1481

model	parameters	r_s^{Planck}	r_s^{WMAP}	$r_s^{Nunes\,et\,al.\,(2020a)}$
ΛCDM	Ω_m	0.481 ± 0.140	0.408 ± 0.115	0.448 ± 0.128
	Ω_Λ	0.608 ± 0.233	0.532 ± 0.194	0.578 ± 0.217
	r_s	98.858 ± 2.362	106.605 ± 0.537	102.014 ± 2.227
	χ^2_{reduced}	1.026	1.028	1.027
wCDM	Ω_m	0.469 ± 0.157	0.417 ± 0.125	0.427 ± 0.153
	w	-1.083 ± 0.499	-1.152 ± 0.484	-1.079 ± 0.488
	r_s	98.961 ± 2.301	106.597 ± 0.540	102.002 ± 2.176
	χ^2_{reduced}	1.186	1.170	1.191
$w(t)$CDM	w_0	-0.855 ± 0.368	-1.194 ± 0.244	-1.000 ± 0.321
	w_1	-0.111 ± 0.562	-0.012 ± 0.573	-0.059 ± 0.569
	r_s	99.253 ± 2.187	106.556 ± 0.533	101.980 ± 2.100
	χ^2_{reduced}	1.247	1.136	1.167

Table 2. Constrained parameters for the models ΛCDM, wCDM, and $w(t)$CDM considering the sound horizon scale, r_s, given by the Planck Collaboration (2020), WMAP Hinshaw et al. (2013), and Nunes et al. (2020a). The units for the values of r_s are Mpc/h.

Barboza, E., & Alcaniz, J. S. 2008, Phys. Lett. B, 666, 415

Bassett, B., & Hlozek, R. 2010, Baryon acoustic oscillations, in Dark Energy: Observational and Theoretical Approaches, Cambridge Univ. Press, p. 246

Bengaly, C. A. P., Bernui, A., Ferreira, I. S., Alcaniz, J. S. 2017, MNRAS, 466, 2799

Beutler, F., Blake, C., Colless, M., et al. 2011, MNRAS, 416, 3017

Blake, C., Kazin, E. A., Beutler, F., et al. 2011, MNRAS, 418, 1707

Bond, J. R., & Efstathiou, G. 1987, MNRAS, 226, 655

Carnero, A., Sánchez, E., Crocce, M., Cabré, A., & Gaztanaga, E. 2012, MN-RAS, 419, 1689

Carter, P., Beutler, F., Percival W. J., et al. 2018, MNRAS, 481, 2371

Carvalho, G. C., Bernui A., Benetti, M., Carvalho, J. C., & Alcaniz, J. S. 2016, Phys. Rev. D, 93, 023530

Carvalho, G. C., Bernui, A., & Benetti, M., et al. 2020, Astroparticle Physics, 119, 102432, arXiv:1709.00271

Challinor, A., & Lewis, A. 2011, Phys. Rev. D, 84, 043516

Cole, S., Percival, W. J., Peacock, J. A., et al. 2005, MNRAS, 362, 505

de Carvalho, E., Bernui, A., Carvalho, G. C., Novaes, C. P., & Xavier, H. S. 2018, J. Cosmology Astropart. Phys., 04, 064

de Carvalho, E., Bernui, A., Xavier, H. S., & Novaes, C. P. 2020, MNRAS, 492, 4469

Eisenstein, D. J., & Hu, W. 1998, ApJ, 496, 605

Eisenstein, D. J., Zehavi, I., Hogg, D. W., et al. 2005, ApJ, 633, 560

Eisenstein, D. J., Seo, H.-J., & White, M. 2007, ApJ, 664, 660

Feldbrugge, J., van Engelen, M., van de Weygaert, R., Pranav, P., & Vegter, G. 2019, J. Cosmology Astropart. Phys., 09, 052

Feldman, H. A., Kaiser, N., & Peacock, J. A. 1994, ApJ, 426, 23

Foreman-Mackey, D. 2016, The Journal of Open Source Software, 1

Górski, K. M., Hivon, E., Banday, A. J., et al. 2005, ApJ, 622, 759

Hinshaw, G., Larson D., Komatsu E., et al. 2013, ApJS, 208, 19

Jarvis, M., Bernstein, G., & Jain, B. 2004, MNRAS, 352, 338

Kaiser, N. 1987, MNRAS, 227, 1

Landy, S. D., & Szalay, A. S. 1993, ApJ, 412, 64

Marques, G. A., et al. 2019, J. Cosmology Astropart. Phys., 06, 019, arXiv:1812.08206

Marques, G. A., & Bernui A. 2020a, J. Cosmology Astropart. Phys., 05, 052, arXiv:1908.04854

Marques, G. A., Liu, J., Huffenberger, K. M., Colin H. J. 2020b, ApJ, 904, 182, arXiv:2008.04369

Novaes, C. P., Bernui, A., Marques, G. A., & Ferreira, I. S. 2016, MNRAS, 461, 1363

Novaes, C. P., Bernui, A., Xavier, H. S., & Marques, G. A. 2018, MNRAS, 478, 3253

Nunes, R. C., Yadav, S. K., Jesus, J. F., & Bernui, A. 2020a, MNRAS, 497, 2, arXiv:2002.09293

Nunes, R. C., & Bernui, A. 2020b, EPJC, 80, 1025, arXiv:2008.03259

Pandey, B., & Sarkar, S. 2020, MNRAS, 498, 6069, arXiv:2002.08400

Peebles, P. J. E., & Hauser, M. G. 1974, ApJS, 28, 19

Peebles, P. J. E., & Yu J. T. 1970, ApJ, 162, 815

Planck Collaboration, Aghanim N., Akrami, Y., Ashdown, M., et al. 2020, A&A 641, A6, arXiv:1807.06209

Salazar-Albornoz, S., Sánchez, A. G., Grieb, J. N. et al. 2017, MNRAS, 468, 2938

Sánchez, E. , Carnero, A., Garcia-Bellido, J. et al. 2011, MNRAS, 411, 277

Sosa Nuñez, F., Niz, G. 2020, J. Cosmology Astropart. Phys., 12, 021

Sunyaev, R. A., & Zeldovich, Y. B. 1970, Astrophysics and Space Science, 7, 3

Xavier, H. S., Abdalla, F. B., & Joachimi, B. 2016, MNRAS, 459, 3693

York, D. G., Adelman, J., Anderson, J. E., et al. 2000, AJ, 120, 1579